Editors' Suggestion

Quantum control and noise protection of a Floquet 0-π qubit

Zhaoyou Wang [1,*] and Amir H. Safavi-Naeini [1,2,†]

[1] *E. L. Ginzton Laboratory and the Department of Applied Physics, Stanford University, Stanford, California 94305, USA*

[2] *AWS Center for Quantum Computing, Pasadena, California 91125, USA*

(Received 17 February 2024; accepted 14 March 2024; published 3 April 2024)

Time-periodic systems allow engineering new effective Hamiltonians from limited physical interactions. For example, the inverted position of the Kapitza pendulum emerges as a stable equilibrium with rapid drive of its pivot point. In this work we propose the Kapitzonium: a Floquet qubit that is the superconducting circuit analog of a mechanical Kapitza pendulum. Under periodic driving, the bit- and phase-flip rates of the emerging qubit states are exponentially suppressed with respect to the ratio of the effective Josephson energy to charging energy. However, we find that dissipation causes leakage out of the Floquet qubit subspace. We engineer a passive cooling scheme to stabilize the qubit subspace, which is crucial for high-fidelity quantum control under dissipation. Furthermore, we introduce a hardware-efficient fluorescence-based method for qubit measurement and discuss the experimental implementation of the Floquet qubit. Our work provides the fundamental steps to develop more complex Floquet quantum systems from the ground up to realize large-scale protected engineered dynamics.

DOI: 10.1103/PhysRevA.109.042607

I. INTRODUCTION

Superconducting circuits offer flexible qubit designs, which hold promise for engineering scalable quantum computers [1–11]. Quantum information is encoded in eigenstates of the circuit, and qubit properties can be engineered with different circuit designs. Single-mode circuits such as the transmon and fluxonium have demonstrated long coherence times and high gate fidelity [1–4]. In addition, their ease of fabrication and manipulability make them popular choices as qubits. More complex multimode circuits have been proposed, such as the 0-π qubit [5], which in theory provide a greater level of protection against decay and dephasing. The intrinsic noise protection of these circuits comes from engineering two degenerate ground states with disjoint wave functions [12,13]. Many local noise processes are significantly suppressed by these types of states. However, the protected qubits usually require circuit parameters that are demanding for current experiments [6,12,13].

Alternative and less demanding approaches to realizing circuit-level noise protection have emerged over the past decade. In these approaches, time modulation of the superconducting circuit is used to engineer a subspace that is protected against either bit flips or phase flips or both. Prominent examples of these schemes include the dissipative cats [14–16], Kerr cats [17,18], and recent proposals and implementations of autonomously corrected qubits [19–21]. In all of these works, the modulation frequencies and amplitudes are tuned to induce a certain set of transitions, with the notable exception of Ref. [21], where a Gottesman-Kitaev-Preskill qubit is stabilized by modulating the Josephson circuit with a microwave frequency comb. The drive amplitudes are usually much weaker than the Josephson energy, resulting in qubit states localized around the single Josephson potential minimum.

Here we propose a qubit design based on circuits whose Josephson potentials are strongly modulated in time. The modulation frequency does not have to align with any particular transitions, simplifying the handling of ac Stark effects in the presence of multiple strong drives [20]. In general, the dynamics of a time-periodic system is governed by the effective Hamiltonian from the Floquet theory [22,23]. Engineering the Floquet Hamiltonian enables new designs of superconducting qubits [24–26]. The Floquet qubit we study is the superconducting circuit analog to the mechanical Kapitza pendulum [27]. In the Kapitza pendulum, the pivot point of the pendulum is periodically moved up and down [Fig. 1(a)], leading to qualitatively new dynamics. Notably, the Kapitza pendulum has two stable equilibria: one at $\phi = 0$ and the other at $\phi = \pi$, where ϕ is the angle relative to the vertical downward position of the pendulum. In the qubit that we propose here, superpositions of the $\phi = 0$ and $\phi = \pi$ configurations make up the logical subspace of the qubit. We thus name this Floquet 0-π qubit the Kapitzonium. Note that the quantum Kapitza pendulum along with its connection to protected superconducting qubits has been studied in Ref. [23]. In this paper we focus on the quantum control and noise protection of the Kapitzonium.

Our paper is organized as follows. In Sec. II we introduce the Kapitzonium and its unitary gates. In Sec. III we consider the open-system dynamics of the Kapitzonium where heating effects induced by charge noise are suppressed with engineered cooling. In Sec. IV we discuss some technical aspects

*Present address: Pritzker School of Molecular Engineering, University of Chicago, Chicago, Illinois 60637, USA; zhaoyou@uchicago.edu

†safavi@stanford.edu

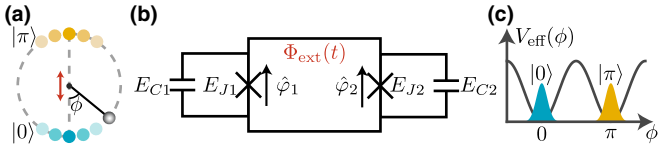

FIG. 1. Schematics of the Kapitzonium. (a) Kapitza pendulum. (b) Superconducting circuit implementing the Kapitzonium. (c) Effective double-well potential showing the disjoint wave functions and degeneracy of $|0\rangle$ and $|\pi\rangle$.

of the experimental implementation of the Kapitzonium. In Sec. V we conclude our discussion with potential directions for future study.

II. UNITARY DYNAMICS OF THE KAPITZONIUM

A. Kapitzonium Hamiltonian

The Kapitzonium circuit [Fig. 1(b)] is identical to that of a capacitively shunted superconducting quantum interference device (SQUID). The external flux $\Phi_{\rm ext}(t)$ threading the SQUID loop is used to emulate the effect of a time-modulated pivot point of a pendulum. The Kapitzonium Hamiltonian is derived with the established circuit quantization procedures [28–31]. The branch flux variable $\hat{\varphi}_k$ across each Josephson junction and the conjugate charge variable $\hat{n}_k$ satisfy $[\hat{\varphi}_k, \hat{n}_k] = i$ for $k = 1, 2$. The circuit Hamiltonian is

$$\hat{H} = \sum_{k=1,2} 4E_{Ck}\hat{n}_k^2 - E_{Jk}\cos\hat{\varphi}_k, \tag{1}$$

where E_{Jk} are the Josephson energies and $E_{Ck} = e^2/2C_k$ are the charging energies, with C_k the sum of junction capacitance and shunt capacitance.

Flux quantization sets the constraint of $\hat{\varphi}_1 - \hat{\varphi}_2 = \Phi_{\rm ext}(t)$. In the symmetric case of $E_{J1} = E_{J2}$ and $E_{C1} = E_{C2}$, Eq. (1) reduces to the Kapitzonium Hamiltonian

$$\hat{H}(t) = 4E_C\hat{n}^2 - E_J\cos\phi_{\rm ext}(t)\cos\hat{\phi}, \tag{2}$$

where $\phi_{\rm ext}(t) = \Phi_{\rm ext}(t)/2$. The flux variable $\hat{\phi} = (\hat{\varphi}_1 + \hat{\varphi}_2)/2$ corresponds to the pendulum rotation angle and $\hat{n} = \hat{n}_1 + \hat{n}_2$ is the conjugate charge variable satisfying $[\hat{\phi}, \hat{n}] = i$. The charging energy is $E_C = e^2/2(C_1 + C_2)$ and the Josephson energy is $E_J = E_{J1} + E_{J2}$.

To realize the analog of the Kapitza pendulum, we set the external flux to $\phi_{\rm ext}(t) = \omega t$. The idling dynamics is described by a Floquet Hamiltonian

$$\hat{H}_0(t) = 4E_C\hat{n}^2 - E_J\cos\omega t\cos\hat{\phi} \tag{3}$$

with a time period of $T = 2\pi/\omega$. The effective Hamiltonian of $\hat{H}_0(t)$ has been derived in Ref. [23] and is given by

$$\hat{H}_{\rm eff} = 4E_C\hat{n}^2 - \tilde{E}_J\cos 2\hat{\phi} \tag{4}$$

up to the second order, where $\tilde{E}_J = E_C E_J^2/\omega^2$. Throughout this paper, we choose Kapitzonium parameters $E_J/2\pi = 100$ GHz, $\omega/2\pi = 10$ GHz, and $E_C/2\pi = 0.01$ GHz unless specified otherwise. Such a parameter choice guarantees that higher-order terms can be neglected where the third-order term is 0 and the fourth-order term scales as $E_C^3E_J^2/\omega^4 \ll \tilde{E}_J$ [22,23]. Since $\hat{\phi}$ is 2π periodic, $\hat{H}_{\rm eff}$ has two near-degenerate ground states $(|0\rangle \pm |\pi\rangle)/\sqrt{2}$ in the deep transmon regime of $\tilde{E}_J/E_C = 100$. Here $|0\rangle$ and $|\pi\rangle$ are localized at the two minima of the effective potential $V_{\rm eff}(\phi) = -\tilde{E}_J\cos 2\phi$ [Fig. 1(c)] with exponentially small overlap.

We can understand the noise protection of the Kapitzonium intuitively from the effective Hamiltonian. Since only two Cooper pairs tunneling is allowed by $\cos 2\hat{\phi}$, one ground state belongs to the even Cooper pair subspace while the other belongs to the odd Cooper pair subspace. The distinct parities of the two ground states hold even in the presence of the offset charge n_g, modeled by replacing $\hat{n}$ with $\hat{n} - n_g$. As a result, the charge operator $\hat{n}$ does not couple the two ground states. Furthermore, the ground-state wave functions are delocalized in the charge space since $\tilde{E}_J/E_C \gg 1$, leading to exponentially suppressed charge dispersion in n_g with $\sqrt{\tilde{E}_J/E_C} = E_J/\omega$, similar to the usual transmon [3]. For more discussion of the coherence properties of the Kapitzonium, refer to Sec. IV C.

B. Floquet eigenstates

The effective Hamiltonian provides a useful approximate picture of the potential and the "ground" states of the Kapitzonium; note that the states $(|0\rangle \pm |\pi\rangle)/\sqrt{2}$ are only the ground states of the effective Hamiltonian. To better understand the states, gates, and noise, we need to move beyond the effective description and consider the Floquet eigenstates of the qubit. The Floquet eigenstates $|\Psi_\alpha(t)\rangle$ of the idling Kapitzonium Hamiltonian $\hat{H}_0(t)$ satisfy

$$\hat{H}_0(t)|\Psi_\alpha(t)\rangle = i\frac{d}{dt}|\Psi_\alpha(t)\rangle \tag{5}$$

and have the form

$$|\Psi_\alpha(t)\rangle = e^{-i\varepsilon_\alpha t}|\Phi_\alpha(t)\rangle. \tag{6}$$

Here $|\Phi_\alpha(t)\rangle = |\Phi_\alpha(t+T)\rangle$ are the periodic Floquet modes and ε_α are the Floquet eigenenergies.

We can calculate the Floquet eigenenergies and eigenstates to verify the double-well nature of the effective potential. Here the indices α are sorted based on the overlaps between $|\Psi_\alpha(t=0)\rangle$ and the eigenstates of $\hat{H}_{\rm eff}$. In Fig. 2(a) we find a close match between the exact Floquet eigenenergies ε_α and the spectrum of $\hat{H}_{\rm eff}$, and the lowest few eigenstates form near degenerate two-level manifolds with $\varepsilon_{2k} \approx \varepsilon_{2k+1}$ for $k = 0, 1, 2$. Within each manifold, we define the Floquet modes $|\Phi_k^+(t)\rangle \equiv |\Phi_{2k}(t)\rangle$ and $|\Phi_k^-(t)\rangle \equiv |\Phi_{2k+1}(t)\rangle$, where $+$ and $-$ represent whether the wave function has the same or opposite sign in the 0 well and π well. In Fig. 2(b) we plot the localized Floquet modes defined as

$$\begin{aligned}|\Phi_k^0(t)\rangle &= \frac{1}{\sqrt{2}}[|\Phi_k^+(t)\rangle + |\Phi_k^-(t)\rangle],\\ |\Phi_k^\pi(t)\rangle &= \frac{1}{\sqrt{2}}[|\Phi_k^+(t)\rangle - |\Phi_k^-(t)\rangle],\end{aligned} \tag{7}$$

where $|\Phi_k^0(t)\rangle$ and $|\Phi_k^\pi(t)\rangle$ are localized in the 0 well and π well, respectively.

In contrast to the eigenstates of a static Hamiltonian, Floquet modes are not stationary but periodic in time. Figure 2(c) shows the ϕ space probability distributions of the localized Floquet modes $|\Phi_0^0(t)\rangle$ and $|\Phi_0^\pi(t)\rangle$. The rapidly inverting

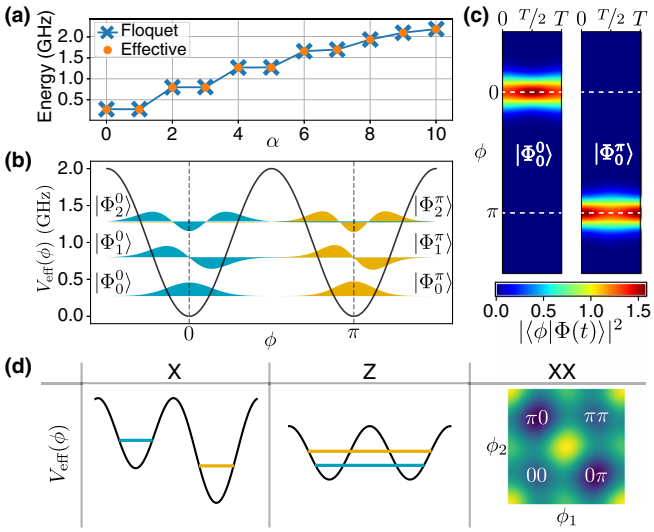

FIG. 2. (a) Floquet eigenenergies of $\hat{H}_0(t)$ compared with the spectrum of $\hat{H}_{\rm eff}$. The energy splitting in the ground-state manifold is $(\varepsilon_1-\varepsilon_0)/2\pi \approx 4.7$ kHz, which is much smaller than the gap between the ground and first excited manifolds. (b) Localized Floquet modes $|\Phi_k^0(t)\rangle$ and $|\Phi_k^\pi(t)\rangle$ at $t=0$ for $k=0,1,2$. (c) Probability distributions of the localized Floquet modes $|\Phi_0^0(t)\rangle$ and $|\Phi_0^\pi(t)\rangle$ from 0 to T in the ϕ space. (d) Effective potential when performing different gates.

$\cos\phi$ potential causes $\phi=0$ and π to alternate between being stable or unstable equilibrium points, driving oscillations in the spreads of the wave functions. Such oscillations are neglected in the effective Hamiltonian description but induce heating despite a zero-temperature bath, as we discuss in Sec. III.

A single-qubit state (c_0, c_1) can be encoded in the Kapitzonium as

$$|\psi(t)\rangle = c_0|\Psi_0(t)\rangle + c_1|\Psi_1(t)\rangle, \tag{8}$$

where c_0 and c_1 are invariant under $\hat{H}_0(t)$. For $(\varepsilon_1-\varepsilon_0)/2\pi \approx 4.7$ kHz, $1/(\varepsilon_1-\varepsilon_0)$ is much longer than the timescale of any relevant Kapitzonium operations. We thus assume $\varepsilon_0=\varepsilon_1$ and only consider the system at $t=nT$ to simplify our discussion. In this case, the qubit basis states $|\Psi_0\rangle$ and $|\Psi_1\rangle$ become static and are related to $|0\rangle$ and $|\pi\rangle$ by the transformations

$$|\Psi_0\rangle = \frac{1}{\sqrt{2}}(|0\rangle + |\pi\rangle),$$
$$|\Psi_1\rangle = \frac{1}{\sqrt{2}}(|0\rangle - |\pi\rangle). \tag{9}$$

Note that the $|0\rangle$ state can be initialized by starting from the ground state of a transmon and then adiabatically turning on the Floquet drive (see Appendix B).

C. Kapitzonium gates

The encoded qubit state can be manipulated by engineering the flux drive $\phi_{\rm ext}(t)$. The resulting effective potentials [Fig. 2(d)] provide the intuition for the Kapitzonium gates. Here we focus on the gate Hamiltonians and details on the required flux drive are discussed in Sec. IV.

1. The X rotation

The X gate Hamiltonian $\hat{H}_x(t) = \hat{H}_0(t) + \alpha_x \cos\hat{\phi}$ generates the rotation along the X axis. The effective potential now becomes an asymmetric double well $V_{\rm eff}^{(x)}(\phi) = -\tilde{E}_J\cos 2\phi + \alpha_x\cos\phi$, which lifts the degeneracy between $|0\rangle$ and $|\pi\rangle$. Therefore, we have $\hat{H}_x(t) \approx \alpha_x(|0\rangle\langle 0| - |\pi\rangle\langle\pi|) = \alpha_x\hat{\sigma}_x$ in the $\{|\Psi_0\rangle, |\Psi_1\rangle\}$ basis, leading to Rabi oscillation between $|\Psi_0\rangle$ and $|\Psi_1\rangle$.

2. The Z rotation

The depth $\tilde{E}_J$ of the effective double-well potential can be controlled dynamically with the flux driving frequency ω. Increasing ω reduces $\tilde{E}_J/E_C = (E_J/\omega)^2$ and induces stronger coupling between $|0\rangle$ and $|\pi\rangle$. We choose $\omega_z/2\pi = 20$ GHz for the Z gate, which lifts the degeneracy between $|\Psi_0\rangle$ and $|\Psi_1\rangle$ with a splitting $(\varepsilon_1-\varepsilon_0)/2\pi \approx 1.8$ MHz. This implements a phase gate for $|\Psi_0\rangle$ and $|\Psi_1\rangle$, i.e., the rotation along the Z axis.

3. Two-qubit XX rotation

We couple two Kapitzoniums with a Josephson junction to realize the XX gate Hamiltonian $\hat{H}_{xx}(t) = \hat{H}_0(t) + \alpha_{xx}\cos(\hat{\phi}_1 - \hat{\phi}_2)$. Replacing the Josephson junction with a SQUID makes the coupling tunable. The joint effective potential is $V_{\rm eff}^{(xx)}(\phi_1,\phi_2) = -\tilde{E}_J\cos 2\phi_1 - \tilde{E}_J\cos 2\phi_2 + \alpha_{xx}\cos(\phi_1-\phi_2)$, which lifts the degeneracy between $\{|00\rangle, |\pi\pi\rangle\}$ and $\{|0\pi\rangle, |\pi 0\rangle\}$. Therefore, we have $\hat{H}_{xx}(t) \approx \alpha_{xx}(|00\rangle\langle 00| + |\pi\pi\rangle\langle\pi\pi| - |0\pi\rangle\langle 0\pi| - |\pi 0\rangle\langle\pi 0|) = \alpha_{xx}\hat{\sigma}_x \otimes \hat{\sigma}_x$ in the $\{|\Psi_0\rangle, |\Psi_1\rangle\}$ basis, generating the XX rotation.

III. OPEN-SYSTEM DYNAMICS OF KAPITZONIUM

A. Heating problem

In an open quantum system, a coupling between the system and bath allows the bath to induce transitions between different eigenstates of the system. Both the form of the coupling and the temperature of the bath go into determining the transitions and their rates. For simplicity, we consider only a zero-temperature bath in this paper. For time-independent systems, any transition from lower to higher energy will require energy to be absorbed from the bath. Because of this, static systems coupled to zero-temperature baths eventually decay to their ground states.

Considering the level structure in Fig. 2(b), we would naively expect the zero-temperature bath to induce only the downward transition $|\Psi_2\rangle \to |\Psi_0\rangle$, with the opposing transition $|\Psi_0\rangle \to |\Psi_2\rangle$ being suppressed as that would require absorption of energy from the bath. This intuition is incorrect because the Kapitzonium is a Floquet system, which is constantly exchanging energy with the Floquet drive. As a result, the bath-induced transitions happen in both directions between the Floquet eigenstates: Both $|\Psi_2\rangle \to |\Psi_0\rangle$ and $|\Psi_0\rangle \to |\Psi_2\rangle$ transitions are allowed in a Kapitzonium interacting with a zero-temperature bath. Therefore, in contrast to the static 0-π qubit [5], the Floquet $|0\rangle$ and $|\pi\rangle$ can still decay out of the qubit subspace through what looks like a heating process.

Consider a generic Floquet system $\hat{H}_0(t) = \hat{H}_0(t+T)$ coupled to some bath degrees of freedom $\hat{B}(t)$ via the

system operator $\hat{O}$. The system-bath Hamiltonian in the rotating frame of the bath is

$$\hat{H}_{\mathrm{SB}}(t) = \hat{H}_0(t) + \hat{O}\hat{B}(t), \tag{10}$$

where

$$\hat{B}(t) = \sum_k g_k(\hat{b}_k e^{-i\omega_k t} + \hat{b}_k^\dagger e^{i\omega_k t}). \tag{11}$$

Here $\omega_k \geqslant 0$ is the frequency of the kth bath mode and g_k is the coupling between the kth mode and the system.

The emission spectrum of the Floquet system can be calculated in the interaction picture of $\hat{H}_0(t)$. More specifically, the unitary $\hat{U}_0(t)$ generated by $\hat{H}_0(t)$ is given by

$$\hat{U}_0(t, t_0) = \sum_\alpha |\Psi_\alpha(t)\rangle\langle\Psi_\alpha(t_0)|, \tag{12}$$

where $|\Psi_\alpha(t)\rangle$ are the Floquet eigenstates of $\hat{H}_0(t)$, and $\hat{U}_0(t, t_0)$ satisfies the Schrödinger equation

$$i\frac{d}{dt}\hat{U}_0(t, t_0) = \hat{H}_0(t)\hat{U}_0(t, t_0). \tag{13}$$

Now we could perform the unitary transformation $\hat{U}_0(t, t_0)$, and the system-bath Hamiltonian in the interaction picture becomes

$$\tilde{H}_{\mathrm{SB}}(t) = \hat{O}(t)\hat{B}(t), \tag{14}$$

where

$$\hat{O}(t) = \hat{U}_0^\dagger(t, t_0)\hat{O}\hat{U}_0(t, t_0) = \sum_{\alpha\beta} O_{\alpha\beta}(t)|\Psi_\alpha(t_0)\rangle\langle\Psi_\beta(t_0)|, \tag{15}$$

with $O_{\alpha\beta}(t) = \langle\Psi_\alpha(t)|\hat{O}|\Psi_\beta(t)\rangle$. We set $t_0 = 0$ without loss of generality.

Since the Floquet modes $|\Phi_\alpha(t)\rangle$ are periodic in time, we Fourier expand $O_{\alpha\beta}(t)$,

$$\begin{aligned} O_{\alpha\beta}(t) &= e^{i(\varepsilon_\alpha - \varepsilon_\beta)t}\langle\Phi_\alpha(t)|\hat{O}|\Phi_\beta(t)\rangle \\ &= e^{i(\varepsilon_\alpha - \varepsilon_\beta)t}\sum_{n=-\infty}^{\infty} O_{\alpha\beta n}e^{in\omega t}, \end{aligned} \tag{16}$$

where $O_{\alpha\beta n}$ together with $\{\varepsilon_\alpha\}$ gives the emission spectrum. Since all $\hat{b}_k$ modes are in vacuum, the transition $\alpha \to \beta$ from $|\Psi_\alpha(t_0)\rangle$ to $|\Psi_\beta(t_0)\rangle$ is only possible if $\varepsilon_\alpha - \varepsilon_\beta + n\omega > 0$, with the transition rate determined by $|O_{\alpha\beta n}|^2$ and the bath spectral density at frequency $\varepsilon_\alpha - \varepsilon_\beta + n\omega$. Furthermore, the transition $\alpha \to \beta$ could emit photons at multiple frequencies and both $\alpha \to \beta$ and $\beta \to \alpha$ could occur, which is different from the relaxation of static systems.

In Fig. 3(a) we plot $|O_{\alpha\beta n}|^2$ for various transitions of the Kapitzonium under charge noise with $\hat{O} = \hat{n}$. The dominant heating processes $0 \to 2$ (red cross) and $1 \to 3$ (red dot) occur at near-degenerate frequency around $\omega_{02}/2\pi \approx \omega_{13}/2\pi \approx 9.5$ GHz. The reverse cooling processes $2 \to 0$ (blue cross) and $3 \to 1$ (blue dot) are also allowed at a different frequency around $\omega_{20}/2\pi \approx \omega_{31}/2\pi \approx 10.5$ GHz.

Assuming the bath spectral density is flat, we trace out the bath degrees of freedom and derive a master equation for the Kapitzonium. In the interaction picture, the master equation is $\dot{\hat{\rho}} = \kappa D[\hat{O}_-(t)](\hat{\rho})$ (see Appendix A), where

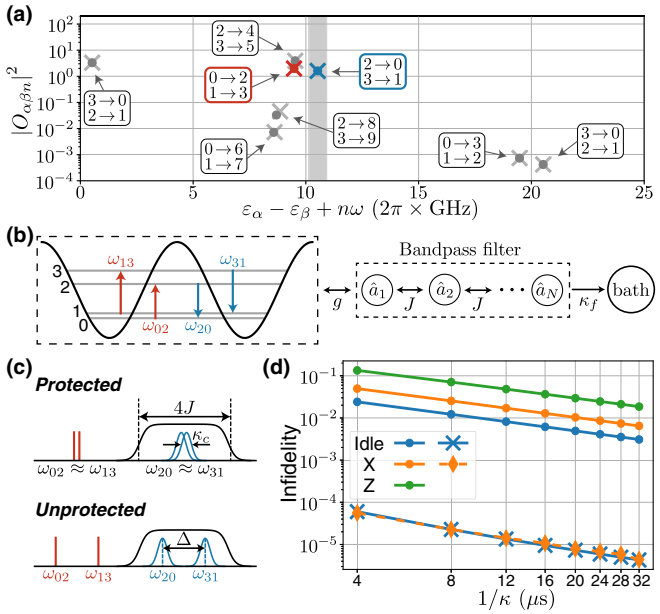

FIG. 3. (a) Emission spectrum of the Kapitzonium under charge noise. The upper (lower) $m \to n$ label within each rounded rectangle corresponds to the cross (dot). Only transitions involving $|\Psi_{0\text{–}3}\rangle$ with emission frequencies less than 25 GHz are shown here. (b) Schematic for the Kapitzonium coupled to a bandpass filter. (c) Two different regimes of the emission spectrum, which determines whether the qubit can be protected or not. (d) Idling and gate fidelity for different intrinsic loss rate κ, with (crosses and diamonds) and without (dots) the filter.

$D[\hat{A}](\hat{\rho}) = \hat{A}\hat{\rho}\hat{A}^\dagger - \frac{1}{2}\{\hat{A}^\dagger\hat{A}, \hat{\rho}\}$. Here κ is the intrinsic loss rate and

$$\hat{O}_-(t) = \sum_{\alpha\beta} O^-_{\alpha\beta}(t)|\Psi_\alpha(t_0)\rangle\langle\Psi_\beta(t_0)|, \tag{17}$$

where

$$O^-_{\alpha\beta}(t) = e^{i(\varepsilon_\alpha - \varepsilon_\beta)t}\sum_{\varepsilon_\alpha - \varepsilon_\beta + n\omega < 0} O_{\alpha\beta n}e^{in\omega t}. \tag{18}$$

Numerically the matrix elements $|O^-_{20}(t)|$ and $|O^-_{31}(t)|$ are of order 1; therefore, the intrinsic loss rate κ is approximately the heating rate from the logical subspace. For a flat bath spectral density, κ also corresponds to the amplitude damping rate of the transmon when the Floquet driving is turned off.

Selection rules

We can derive the selection rules for the Kapitzonium under charge noise to better understand the emission spectrum in Fig. 3(a). The selection rules come from the symmetry of the Floquet modes $|\Phi_\alpha(t)\rangle$ under two different charge parity transformations $\hat{\Pi}_1 = \sum_n |-n\rangle\langle n|$ and $\hat{\Pi}_2 = \sum_n (-1)^n|n\rangle\langle n|$, where $\{|n\rangle\}$ are the charge eigenstates.

The Kapitzonium Hamiltonian (3) is invariant under $\hat{\Pi}_1$ with $[\hat{\Pi}_1, \hat{H}_0(t)] = 0$; therefore, the Floquet modes are parity eigenstates where $\hat{\Pi}_1|\Phi_\alpha(t)\rangle = (-1)^{\pi_1(\alpha)}|\Phi_\alpha(t)\rangle$, $\pi_1(\alpha) = 0, 1$. The parities $\pi_1(\alpha)$ for the first 12 Floquet modes are given in Table I, which agrees with the eigenstates of $\hat{H}_{\mathrm{eff}}$ under transformation $\hat{\Pi}_1$. The parity is the same within

TABLE I. Parities $\pi_1(\alpha)$ and $\pi_2(\alpha)$ for Floquet modes $|\Phi_\alpha(t)\rangle$ transformed under transformations $\hat{\Pi}_1$ and $\hat{\Pi}_2$.

α	0	1	2	3	4	5	6	7	8	9	10	11
$\pi_1(\alpha)$	0	0	1	1	0	0	1	1	0	0	1	1
$\pi_2(\alpha)$	0	1	1	0	0	1	1	0	0	1	1	0

each two-level manifold, whereas it alternates between even and odd parity for different manifolds. Since $\hat{\Pi}_1\hat{n}\hat{\Pi}_1 = -\hat{n}$, transition between two Floquet eigenstates $|\Psi_\alpha(t)\rangle$ and $|\Psi_\beta(t)\rangle$ is forbidden, i.e., $\langle\Psi_\alpha(t)|\hat{n}|\Psi_\beta(t)\rangle = 0$, if $\pi_1(\alpha) = \pi_1(\beta)$. Therefore, the only allowed transitions are between $\{0, 1, 4, 5, \ldots\}$ and $\{2, 3, 6, 7, \ldots\}$, which agree with the emission spectrum in Fig. 3(a). For example, transitions between $\{2, 3\}$ and $\{0, 1, 4, 5, 8, 9\}$ are allowed while transitions between $\{2, 3\}$ and $\{6, 7, 10, 11\}$ are forbidden.

Furthermore, each allowed transition can happen at multiple frequencies, and we can derive additional selection rules to characterize the emitted photon frequencies from the parity transformation $\hat{\Pi}_2$. Note that $\hat{\Pi}_2\hat{H}_0(t)\hat{\Pi}_2 = \hat{H}_0(t + T/2)$; the transformation of the Floquet modes are therefore given by $\hat{\Pi}_2|\Phi_\alpha(t)\rangle = (-1)^{\pi_2(\alpha)}|\Phi_\alpha(t + T/2)\rangle$, $\pi_2(\alpha) = 0, 1$. The parities $\pi_2(\alpha)$ for the first 12 Floquet modes are given in Table I.

We can Fourier transform the Floquet modes as

$$|\Phi_\alpha(t)\rangle = \sum_{k=-\infty}^{\infty} c_{\alpha k} e^{ik\omega t}|\Phi_{\alpha k}\rangle, \tag{19}$$

which leads to

$$O_{\alpha\beta n} = \sum_{k=-\infty}^{\infty} c^*_{\alpha k} c_{\beta,k+n}\langle\Phi_{\alpha k}|\hat{O}|\Phi_{\beta,k+n}\rangle. \tag{20}$$

The Fourier components $|\Phi_{\alpha k}\rangle$ are parity eigenstates of $\hat{\Pi}_2$:

$$\begin{aligned}\hat{\Pi}_2|\Phi_{\alpha k}\rangle &= \frac{1}{T c_{\alpha k}}\int_0^T dt\, e^{-ik\omega t}\hat{\Pi}_2|\Phi_\alpha(t)\rangle \\ &= (-1)^{\pi_2(\alpha)}\frac{1}{T c_{\alpha k}}\int_0^T dt\, e^{-ik\omega t}|\Phi_\alpha(t + T/2)\rangle \\ &= (-1)^{\pi_2(\alpha)+k}|\Phi_{\alpha k}\rangle.\end{aligned} \tag{21}$$

Since $\hat{\Pi}_2\hat{n}\hat{\Pi}_2 = \hat{n}$, for charge noise $\hat{O} = \hat{n}$ we have

$$[1 - (-1)^{\pi_2(\alpha)+\pi_2(\beta)+n}]O_{\alpha\beta n} = 0. \tag{22}$$

Therefore, $2 \mid \pi_2(\alpha) + \pi_2(\beta) + n$ is a necessary condition to have $O_{\alpha\beta n} \neq 0$. For example, the transitions $0 \leftrightarrow 2$ and $1 \leftrightarrow 3$ can only emit photons at odd n, such as the emissions around 10 GHz with $n = 1$ [Fig. 3(a)]. On the other hand, the transitions $0 \leftrightarrow 3$ and $1 \leftrightarrow 2$ can only emit photons at even n, such as the emissions around 0 and 20 GHz with $n = 0$ and 2 [Fig. 3(a)].

To summarize, the selection rules for the Kapitzonium under charge noise are (i) the transition between two Floquet eigenstates $|\Psi_\alpha(t)\rangle$ and $|\Psi_\beta(t)\rangle$ is only possible if $\pi_1(\alpha) + \pi_1(\beta) = 1$ and (ii) for each allowed transition, photon emission at frequency $n\omega \pm (\varepsilon_\alpha - \varepsilon_\beta)$ is only possible if $2 \mid \pi_2(\alpha) + \pi_2(\beta) + n$.

B. Enhanced cooling with a filter

The frequency dependence of the cavity emission suggests that we can enhance a specific transition rate by increasing the bath's spectral density at the transition frequency [32,33]. More concretely, we propose to capacitively couple the Kapitzonium to a bandpass filter around 10.5 GHz with 800 MHz bandwidth [Fig. 3(a) gray shaded region]. The bandpass filter enhances the cooling processes without causing extra heating, which preserves the qubit basis states $\{|\Psi_0\rangle, |\Psi_1\rangle\}$. Furthermore, the environment cannot distinguish whether the emitted photon comes from the $2 \to 0$ or $3 \to 1$ transition since $\omega_{20} \approx \omega_{31}$. Therefore, the phase coherence between $|\Psi_0\rangle$ and $|\Psi_1\rangle$ is also preserved by the cooling processes, enabling fully autonomous protection of the qubit subspace.

The bandpass filter can be modeled as a chain of linearly coupled harmonic oscillators $\hat{a}_1, \ldots, \hat{a}_N$ [33]. The first filter mode $\hat{a}_1$ also couples capacitively to the Kapitzonium via the interaction $g\hat{n}(\hat{a}_1 + \hat{a}_1^\dagger)$. The full Hamiltonian is [Fig. 3(b)]

$$\begin{aligned}\hat{H}(t) = \hat{H}_0(t) &+ \omega_f\sum_{k=1}^{N}\hat{a}_k^\dagger\hat{a}_k + g\hat{n}(\hat{a}_1 + \hat{a}_1^\dagger) \\ &+ J\sum_{k=1}^{N-1}(\hat{a}_k\hat{a}_{k+1}^\dagger + \hat{a}_k^\dagger\hat{a}_{k+1}),\end{aligned} \tag{23}$$

where ω_f is the center frequency of the filter and J is the coupling rate between two adjacent filter modes. The last filter mode $\hat{a}_N$ decays into a zero-temperature bath at rate κ_f, which is described by the Lindblad dissipator $\kappa_f D[\hat{a}_N]$.

The qubit subspace is autonomously protected when the engineered cooling rate is sufficiently larger than the intrinsic loss rate κ of the Kapitzonium. Following Ref. [33], we choose $N = 3$, $\kappa_f = 2J$, and $g = \kappa_f/5$ such that the filter bandwidth is $2\kappa_f$ and the filter modes are only weakly excited. The cooling rate is about $\kappa_c = 4g^2/\kappa_f = 4\kappa_f/25$ after adiabatically eliminating all filter modes [33–35], which has been derived in the Appendix of Ref. [33]. For $\kappa_f/2\pi = 400\,\text{MHz}$ we have $\kappa_c/2\pi = 64\,\text{MHz}$. In Fig. 3(d) we plot the average fidelity of the Kapitzonium idling for 50 ns with (blue crosses) and without (blue dots) the filter for different values of $1/\kappa$. The cooling enhanced by the filter reduces the idling infidelity by more than two orders of magnitude.

C. Gate protection

The filter that protects idling may not protect the Kapitzonium gates since the emission spectrum could be different during the gates. The filter performance is determined by two quantities of the emission spectrum. One quantity is the frequency spacing $\mathcal{B} \equiv |(\omega_{20} + \omega_{31}) - (\omega_{02} + \omega_{13})|/2$ between the dominant heating and cooling transitions. The $\mathcal{B}$ limits the filter bandwidth κ_f and thus the maximal cooling rate κ_c. The other quantity is the degeneracy of the two heating (cooling) transitions measured by $\Delta \equiv |\omega_{02} - \omega_{13}| = |\omega_{20} - \omega_{31}|$. In the degenerate regime where $\Delta \ll \kappa_c$, such as idling with $\Delta/2\pi \approx 0.2\,\text{MHz}$, the qubit subspace is protected [Fig. 3(c)]. In the nondegenerate regime where $\Delta \gtrsim \kappa_c$, the environment could distinguish which cooling transition the emitted photon comes from and dephase the qubit [Fig. 3(c)]. Therefore, the

qubit basis states $|\Psi_0\rangle$ and $|\Psi_1\rangle$ are protected but not their coherent superpositions.

For the X gate with relatively small $\alpha_x/2\pi \approx 5.2$ MHz, the emission spectrum is similar to the idling emission spectrum. Therefore, the idling filter also protects the X gate, with $\Delta/2\pi \approx 0.8$ MHz well within the degenerate regime.

For the Z gate with $\omega_z/2\pi = 20$ GHz, we have $\mathcal{B}/2\pi \approx 468$ MHz and $\Delta/2\pi \approx 27$ MHz. A different filter is required with center frequency at about 20 GHz. The Z gate is unprotected, since the largest possible cooling rate $4\mathcal{B}/25 \approx 75$ MHz is comparable to Δ.

The full protection of the X gate can be verified numerically, and the gate infidelity is reduced by about two orders of magnitude with the filter [Fig. 3(d), orange diamonds and dots]. The partial protection of the qubit basis states during the Z gate is verified in Appendix B. In principle, the XX gate should also be fully protected for α_{xx} on the order of a few megahertz, since its Δ and $\mathcal{B}$ are similar to those of the X gate. However, we did not simulate the XX gate due to the high computational cost. The simulations are done by first finding the Floquet eigenstates in the charge basis and then transforming into the interaction picture with a cutoff of 30 Floquet eigenstates, keeping all terms with $|O_{\alpha\beta n}|^2 \geqslant 10^{-4}$ in Eq. (16). Following Ref. [33], we choose four basis states for the three filter modes restricted to the zero- and one-excitation manifolds.

The design and noise protection of Kapitzonium gates lead to various factors to consider when choosing the Kapitzonium parameters E_C, E_J, and ω. First, the Z gate requires smaller E_J/ω_z to lower the effective potential well. This sets an upper limit on the permissible value of E_J since otherwise ω_z would exceed the range of current microwave generators. Second, the idling and X gate favor larger E_J/ω, as a deeper effective potential well widens the gap between the ground and first excited manifolds, resulting in larger spacing $\mathcal{B}$ and higher cooling rate κ_c. Finally, $E_C/\omega \ll 1$ is essential to suppress higher-order terms in the effective Hamiltonian (4), and numerically we find $E_C/\omega \sim 10^{-3}$ suitable to preserve the 0-π nature of the Kapitzonium. Given these considerations, we have chosen the parameters $E_J/2\pi = 100$ GHz, $\omega/2\pi = 10$ GHz, and $E_C/2\pi = 0.01$ GHz in Sec. II.

D. Fluorescence-based state measurement

Kapitzonium measurements can be performed by engineering a measurement Hamiltonian $\hat{H}_{\text{meas}}(t)$ with Floquet eigenstates $\{|\Psi'_\alpha\rangle\}$ in the unprotected regime. By measuring the frequency of the emitted photon through the cooling filter, we learn about which transition it comes from and randomly project the system to either $|\Psi'_0\rangle$ or $|\Psi'_1\rangle$ [Fig. 4(a)]. For the X measurement, we choose $\hat{H}_{\text{meas}}(t) = \hat{H}_0(t) + \alpha_x \cos\hat{\phi}$, which is similar to the X gate but with a much larger α_x to lift the degeneracy between ω_{20} and ω_{31}. In this case, $|\Psi'_0\rangle$ and $|\Psi'_1\rangle$ are localized in either well, which corresponds to the measurement basis $\{|0\rangle, |\pi\rangle\}$ [Fig. 4(b)]. On the other hand, we choose $\hat{H}_{\text{meas}}$ as the unprotected Z gate which dephases the qubit and naturally performs the Z measurement with measurement basis $\{|\Psi_0\rangle, |\Psi_1\rangle\}$ [Fig. 4(b)].

The measurement rate is proportional to the occupation of the excited states $|\Psi'_2\rangle$ and $|\Psi'_3\rangle$. We could increase the measurement rate by capacitively driving $|\Psi'_0\rangle \leftrightarrow |\Psi'_2\rangle$ and $|\Psi'_1\rangle \leftrightarrow |\Psi'_3\rangle$ at the heating transition frequency [Fig. 4(a)]. From Eq. (15), the charge operator within the $\{|\Psi'_{0\sim3}\rangle\}$ subspace is

$$\hat{n}(t) = |\Psi'_0\rangle\langle\Psi'_2|(n_{02}e^{i\omega_{02}t} + n_{20}e^{-i\omega_{20}t}) + |\Psi'_1\rangle\langle\Psi'_3|(n_{13}e^{i\omega_{13}t} + n_{31}e^{-i\omega_{31}t}) + \text{H.c.}, \quad (24)$$

where we include only the dominant transitions, and for each transition $n_{\alpha\beta}(t)$ has only one dominant Fourier component (16), which we define as $n_{02} \approx n_{20} \approx n_{13} \approx n_{31} \approx 1$. We apply a charge drive $2\Omega[\cos(\omega_{d1}t) + \cos(\omega_{d2}t)]\hat{n}(t)$ to the Kapitzonium where $\omega_{d1} = \omega_{02}$, $\omega_{d2} = \omega_{13}$, and $\Omega \ll \Delta, \kappa_c$. This leads to the coupling $\Omega(n_{02}|\Psi'_0\rangle\langle\Psi'_2| + n_{13}|\Psi'_1\rangle\langle\Psi'_3| + \text{H.c.})$ after the rotating-wave approximation (RWA). Furthermore, $\{|\Psi'_2\rangle, |\Psi'_3\rangle\}$ are only weakly excited since $\Omega \ll \kappa_c$, which decay back to $\{|\Psi'_0\rangle, |\Psi'_1\rangle\}$ after the measurement with the charge drive turned off.

Kapitzonium measurements can be simulated with quantum trajectory methods [36]. Here we demonstrate the X measurement, while the Z measurement results are similar (see Appendix C). Starting from an initial state of $(|\Psi'_0\rangle + |\Psi'_1\rangle)/\sqrt{2}$, we monitor the output field from the filter with a heterodyne measurement for 2 μs and then calculate the power spectrum $S(\omega)$ for each measurement record $S(t)$. Depending on whether the system is projected into $|\Psi'_0\rangle$ or $|\Psi'_1\rangle$, $S(\omega)$ shows a peak at ω_{20} or ω_{31} [Fig. 4(a)]. We therefore define the signal as $S = S_{31} - S_{20}$, where S_{ij} is the integrated power within a narrow frequency window around ω_{ij}; $S < 0$ or $S > 0$ represents a measurement result of 0 or 1. The measurement

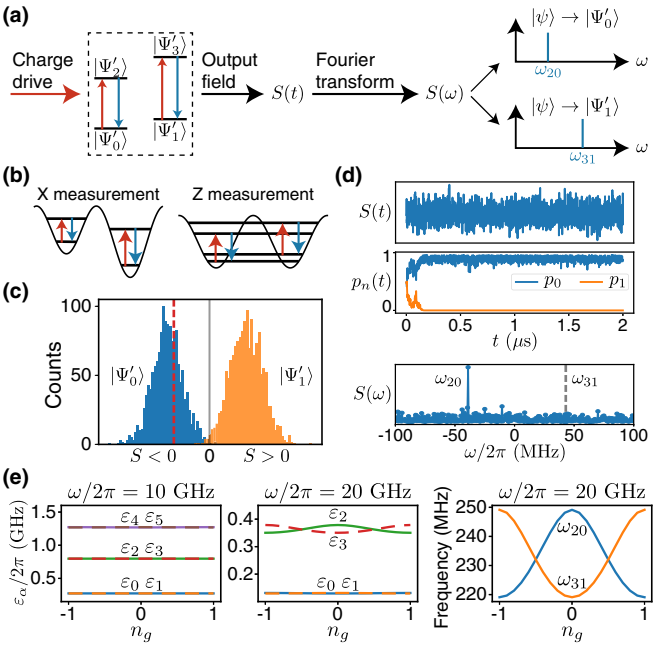

FIG. 4. (a) Kapitzonium measurement by measuring the frequency of the emitted photon. (b) The measurement basis depends on how the degeneracy is lifted between ω_{20} and ω_{31}. (c) Quantum trajectory simulation of the Kapitzonium X measurement. (d) Single trajectory corresponding to the red dashed line in (c), where $S(\omega)$ is plotted in the rotating frame of ω_f. (e) Charge sensitivity of the Floquet eigenenergies and the emission spectrum.

fidelity is about 99.4%, estimated from a total of 3000 trajectories [Fig. 4(c)]. We plot a single trajectory in Fig. 4(d) showing the measurement result $S(t)$, the occupation p_i of $|\Psi_i'\rangle$ during the measurement for $i = 0, 1$, and the spectrum $S(\omega)$.

IV. EXPERIMENTAL IMPLEMENTATION

A. Parameter disorder

Ideally, the SQUID in Fig. 1(b) should be symmetric to engineer the Kapitzonium Hamiltonian (2). However, in actual experiments, there always exists some amount of disorder which requires a more general treatment of the circuit.

The circuit Hamiltonian in the presence of parameter disorder is [29,37]

$$\hat{H}(t) = 4E_C\hat{n}^2 - E_{J1}\cos\left(\hat{\phi} - \frac{C_2}{C_\Sigma}\Phi_{\rm ext}(t)\right) - E_{J2}\cos\left(\hat{\phi} + \frac{C_1}{C_\Sigma}\Phi_{\rm ext}(t)\right), \tag{25}$$

where $C_\Sigma = C_1 + C_2$ is the total junction capacitance and $E_C = e^2/2C_\Sigma$. To symmetrize the flux allocation inside the two cosines, we move to another reference frame by performing the unitary transformation

$$\hat{U} = \exp\left(i\hat{n}\frac{C_2 - C_1}{2C_\Sigma}\Phi_{\rm ext}(t)\right), \tag{26}$$

where the Hamiltonian becomes

$$\hat{H}(t) = 4E_C\hat{n}^2 - E_{J1}\cos\left(\hat{\phi} - \frac{1}{2}\Phi_{\rm ext}(t)\right) - E_{J2}\cos\left(\hat{\phi} + \frac{1}{2}\Phi_{\rm ext}(t)\right) - \frac{C_2 - C_1}{2C_\Sigma}\dot{\Phi}_{\rm ext}(t)\hat{n}. \tag{27}$$

We will drop the unwanted term proportional to $\dot{\Phi}_{\rm ext}(t)\hat{n}$ since in principle it can be compensated for with the gate voltage at the cost of increased control complexity.

For disorder in junction energies, we define $\delta_e = (E_{J1} - E_{J2})/(E_{J1} + E_{J2})$. With the idling flux drive $\phi_{\rm ext}(t) = \omega t$, the effective Hamiltonian is

$$\hat{H}_{\rm eff} = 4E_C\hat{n}^2 - \tilde{E}_J(1 - \delta_e^2)\cos 2\hat{\phi}. \tag{28}$$

Therefore, disorder in junction energies reduces the effective $\tilde{E}_J$, and for small δ_e on the order of 0.05 this reduction is likely negligible.

B. Flux control

Here we discuss the flux control for implementing the Kapitzonium gates and measurements. The flux drives $\phi_{\rm ext}(t) = \omega t$ (idling) and $\phi_{\rm ext}(t) = \omega_z t$ (Z gate and Z measurement) are not feasible experimentally, since the required bias current grows linearly with time. One natural solution is to use a triangle waveform instead

$$\tilde{\phi}_{\rm ext}(t) = \begin{cases} u(t), & 0 \leqslant u(t) < 2\pi \\ 4\pi - u(t), & 2\pi \leqslant u(t) < 4\pi, \end{cases} \tag{29}$$

where $u(t) = \phi_{\rm ext}(t)({\rm mod}4\pi)$. Such a flux choice is exactly equivalent to the ideal flux drives since $\cos[\tilde{\phi}_{\rm ext}(t)] = \cos[\phi_{\rm ext}(t)]$, making $\tilde{\phi}_{\rm ext}(t)$ suitable for implementing idling, the Z gate, and the Z measurement. On the other hand, $\cos[\tilde{\phi}_{\rm ext}(t)]$ has a zero dc component, while a nonzero dc component is necessary for the X gate and X measurement. To achieve a nonzero dc component for $\cos[\tilde{\phi}_{\rm ext}(t)]$, we can choose a triangle waveform with maximal flux $\phi_{\rm max} \neq 2\pi$ such that $\tilde{\phi}_{\rm ext}(t)$ increases from 0 to $\phi_{\rm max}$ and then decreases to 0.

Alternatively, we could set $\phi_{\rm ext}(t) = \alpha\cos\omega t$ with

$$\cos\phi_{\rm ext}(t) = J_0(\alpha) + 2\sum_{n=1}^{\infty}(-1)^n J_{2n}(\alpha)\cos 2n\omega t, \tag{30}$$

where we have applied the Jacobi-Anger expansion and $J_n(x)$ is the nth Bessel function of the first kind. The effective Hamiltonian for Eq. (2) now becomes

$$\hat{H}_{\rm eff} = 4E_C\hat{n}^2 - E_J J_0(\alpha)\cos\hat{\phi} - \tilde{E}_J\sum_{n=1}^{\infty}\left(\frac{J_{2n}(\alpha)}{n}\right)^2\cos 2\hat{\phi}. \tag{31}$$

In principle, we could choose $\alpha = \alpha_0$, where $\alpha_0 \approx 2.4$ is the first zero of $J_0(\alpha)$ for Kapitzonium idling, the Z gate, and the Z measurement, and $\alpha = \alpha_0 + \delta\alpha$ such that $J_0(\alpha) \neq 0$ for the X gate and X measurement. For the X gate, we have $\delta\alpha \approx \alpha_x/E_J J_0'(\alpha_0) \approx 10^{-4}$. However, it may be challenging to achieve a rather large flux modulation α_0 with a precise control over $\delta\alpha$. Furthermore, the multifrequency flux drive [Eq. (30)] may cause unwanted effects beyond the effective Hamiltonian description, which will be left for future explorations.

C. Coherence properties

In this section we give a preliminary discussion of how various noise processes, such as offset charge, flux, and quasiparticle noise, may affect the coherence of the Kapitzonium. Our focus is to qualitatively understand possible effects of the noises, particularly whether or not the qubit subspace and gates are protected. Quantitative estimations and noise mitigation require technical details in implementing the flux control as well as more accurate modeling of the noise processes, which are beyond the scope of the present work.

In the ideal scenario without any imperfections, both the bit-flip rate $1/T_1$ and phase-flip rate $1/T_2$ are 0 since $\langle\Psi_\alpha(t)|\hat{n}|\Psi_\beta(t)\rangle = 0$ for $\alpha, \beta \in \{0, 1\}$ (see Sec. III A). Without cooling, the dominant error is the leakage from the qubit subspace due to the Floquet driving, with a leakage rate $1/T_l \propto \kappa$. The filter implemented in Sec. III suppresses the leakage rate by κ/κ_c, so $1/T_l \propto \kappa^2/\kappa_c$. Such a cooling process also induces dephasing error due to the frequency difference Δ in the emitted photons, with a rate of $1/T_2 \propto \frac{\kappa}{2}(\frac{\Delta}{\kappa_c})^2$. In the deep-potential-well regime $E_J/\omega \gg 1$, we have $\Delta \propto \exp(-\frac{\pi^2 E_J}{8\sqrt{2}\omega})$ and the induced dephasing rate is exponentially small in E_J/ω.

1. Offset charge noise

With a deep potential well $E_J/\omega \gg 1$ during idling, the first few Floquet eigenenergies [Fig. 4(e), left graph] and Floquet eigenstates are insensitive to n_g. Numerically, both

bit-flip and phase-flip rates are exponentially small in E_J/ω with $n_g \neq 0$ (see Appendix D). The weak dependence of the Floquet eigenenergies on n_g also holds when adding $\alpha_x \cos\hat{\phi}$ to the Hamiltonian. Therefore, idling, the X gate, and the X measurement are all insensitive to charge noise.

Due to the shallow potential well, the Z gate and Z measurement are not robust to charge noise where the emitted photon frequencies ω_{20} and ω_{31} depend on n_g [Fig. 4(e), middle and right graphs]. For example, the Z gate and Z measurement cannot be performed at $n_g = 0.5$ where the two cooling transitions emit photons at the same frequency since $\varepsilon_0 = \varepsilon_1$, $\varepsilon_2 = \varepsilon_3$, and $\omega_{20} = \omega_{31}$. This n_g dependence poses challenges to the practical application of the Kapitzonium due to the offset charge drift and charge parity jumps [38,39]. One strategy to mitigate these challenges is to track and correct the Z errors with quantum error correction using, for example, a repetition code.

2. Flux noise

The flux imposed on the loop will be invariably accompanied by additional flux noise $\delta\phi$, which typically has an $f^{-\alpha}$ spectral density [12] and thus a small spectral weight at high frequencies. The effects of $\delta\phi$ depend on how we choose to drive the flux. For $\phi_{\text{ext}}(t) = \omega t + \delta\phi (\text{mod} 4\pi)$, $\delta\phi$ corresponds to a shift in time which does not change the Floquet eigenenergies. Because the idling gate, the Z gate, and the Z measurement can be implemented in this way [Eq. (29)], all these operations are robust to flux noise. However, experimental constraints in implementing a flux drive, as well as the proposed approach to the X gate and X measurement, make other driving schemes such as $\phi_{\text{ext}}(t) = \alpha \cos\omega t$ (Sec. IV B) more attractive. In this case, flux noise leads to an imposed flux of $\phi_{\text{ext}}(t) = \alpha\cos\omega t + \delta\phi$ where $\delta\phi$ has a nontrivial effect on the effective Hamiltonian.

Flux sensitivity at arbitrary flux bias occurs in other protected qubits subject to experimental constraints. For example it is also present in the static soft 0-π qubit [12,13]. Nonetheless, as in the case of the soft 0-π qubit [13], it is possible to operate at a flux sweet spot where the dephasing rate is protected to first order against flux noise. For a Kapitzonium with a noisy periodic flux drive $\phi_{\text{ext}}(t) = \alpha\cos\omega t + \delta\phi$, the effective Hamiltonian is

$$\begin{aligned}\hat{H}_{\text{eff}}(\delta\phi) =& 4E_C\hat{n}^2 - E_J J_0(\alpha)\cos(\delta\phi)\cos\hat{\phi} \\ &- \tilde{E}_J\cos^2(\delta\phi)\sum_{n=1}^{\infty}\left(\frac{J_{2n}(\alpha)}{n}\right)^2\cos 2\hat{\phi} \\ &- 4\tilde{E}_J\sin^2(\delta\phi)\sum_{n=1}^{\infty}\left(\frac{J_{2n-1}(\alpha)}{2n-1}\right)^2\cos 2\hat{\phi}, \quad (32)\end{aligned}$$

which is also insensitive to first order to $\delta\phi$ around $\delta\phi = 0$ with leading-order terms scaling as $\delta\phi^2$. Therefore, operating at the sweet spot $\delta\phi = 0$ can reduce errors of the X gate and X measurement.

3. Quasiparticle noise

Quasiparticle tunneling changes the charge parity. This may induce both energy relaxation and dephasing [3,40–44] of the Kapitzonium. Here we note that in a highly simplified model of quasiparticle dynamics, the frequency shifts in the $\{|0\rangle, |\pi\rangle\}$ basis induced by quasiparticles are proportional to $\langle 0|\sin\frac{\hat{\varphi}_k}{2}|0\rangle \approx (-1)^{k-1}\sin\frac{\phi_{\text{ext}}(t)}{2}$, where $k = 1, 2$ is the index of the junction, and $\langle\pi|\sin\frac{\hat{\varphi}_k}{2}|\pi\rangle \approx \cos\frac{\phi_{\text{ext}}(t)}{2}$. Therefore, for $\phi_{\text{ext}}(t) = \omega t$, $|0\rangle$ and $|\pi\rangle$ on average do not accumulate extra phase and should be robust to quasiparticle tunneling. This analysis may not hold when $\phi_{\text{ext}}(t) = \alpha\cos\omega t$. A more accurate model of quasiparticle tunneling is also likely to be needed to better understand the effects of quasiparticles in the Kapitzonium, such as the photon-assisted effects [45] induced by the modulation drive.

D. Higher harmonics of the Josephson junction

A single $\cos\hat{\phi}$ potential may not be adequate for a precise description of the Josephson junction, and in reality multiple Cooper pairs can tunnel simultaneously, giving rise to higher harmonics of the Josephson potential energy [46]. Here we derive the effective Hamiltonian for the Kapitzonium circuit [Fig. 1(b)], taking into account higher harmonics of the Josephson junctions.

Assuming symmetric circuit parameters, the circuit Hamiltonian is

$$\begin{aligned}\hat{H}(t) &= 4E_C(\hat{n}-n_g)^2 - \sum_{m\geqslant 1}E_{Jm}(\cos m\hat{\varphi}_1 + \cos m\hat{\varphi}_2) \\ &= 4E_C(\hat{n}-n_g)^2 - 2\sum_{m\geqslant 1}E_{Jm}\cos m\omega t\cos m\hat{\phi}, \quad (33)\end{aligned}$$

where $\hat{\phi} = (\hat{\varphi}_1 + \hat{\varphi}_2)/2$, E_{Jm} is the Josephson energy for m Cooper pairs tunneling together, and we have applied the flux quantization condition $\hat{\varphi}_1 - \hat{\varphi}_2 = 2\omega t$. The second-order effective Hamiltonian of Eq. (33) can be derived as [22,23]

$$\hat{H}_{\text{eff}} = 4E_C(\hat{n}-n_g)^2 - \frac{4E_C}{\omega^2}\sum_{m\geqslant 1}(E_{Jm})^2\cos 2m\hat{\phi}, \quad (34)$$

where $\phi = 0, \pi$ are the two degenerate potential minima. Since only an even number of Cooper pairs tunneling is allowed, the two ground states belong to even and odd Cooper pair subspaces, respectively. Furthermore, in the deep-potential-well regime, the charge dispersion in n_g is still exponentially suppressed. In practice, the higher harmonics E_{Jm} $(m > 1)$ are often only a few percent of E_{J1} [46], and we expect the Kapitzonium to be protected in the presence of higher Josephson harmonics.

V. CONCLUSION

We have proposed a quantum Kapitza pendulum in a superconducting circuit as a Floquet 0-π qubit. We identified how single- and two-qubit gates can be implemented and proposed a cooling scheme to protect the Kapitzonium against charge noise. Remarkably, we found that this exceedingly simple Floquet superconducting circuit, a flux-modulated capacitively shunted SQUID loop, can support a protected qubit subspace. Our work revealed some of the subtle features of Floquet qubits: We elucidated the challenges associated with noise-induced heating, as well as how they can be overcome using filter cavities and even used to our advantage to realize a fluorescence-based method for qubit state measurement.

Our work lays the groundwork to study new Floquet systems for quantum information processing with superconducting circuits and outlines a path towards experiments with such devices.

ACKNOWLEDGMENTS

We thank Yudan Guo, Taha Rajabzadeh, Nathan Lee, Takuma Makihara, Qile Su, Jayameenakshi Venkatraman, and Jeremy Boaz Kline for helpful discussions. We also thank the anonymous referees, whose feedback significantly improved this paper. This work was supported by the U.S. government through the Office of Naval Research under Grant No. N00014-20-1-2422 and the National Science Foundation CAREER Award No. ECCS-1941826 and by Amazon Web Services Inc. A.H.S.-N. acknowledges support from the Sloan Fellowship.

APPENDIX A: FLOQUET MASTER EQUATION

In this Appendix we derive the Floquet master equation [47] and the Kapitzonium dissipator. The system-bath Hamiltonian $\hat{H}(t) = \hat{O}(t) \otimes \hat{B}(t)$ in the interaction picture generates the dynamics

$$\begin{aligned}\frac{d}{dt}\hat{\rho}_{SB}(t) &= -i[\hat{H}(t), \hat{\rho}_{SB}(t)] \\ &= -i\left[\hat{H}(t), \hat{\rho}_{SB}(0) - i\int_0^t [\hat{H}(\tau), \hat{\rho}_{SB}(\tau)]d\tau\right] \\ &= -i[\hat{H}(t), \hat{\rho}_{SB}(0)] \\ &\quad - \left[\hat{H}(t), \int_0^t [\hat{H}(\tau), \hat{\rho}_{SB}(\tau)]d\tau\right]. \end{aligned} \tag{A1}$$

Now we make the Born approximation $\hat{\rho}_{SB}(t) = \hat{\rho}(t) \otimes \hat{\rho}_B$, where $\hat{\rho}(t)$ is the system density matrix and $\hat{\rho}_B$ is the stationary bath density matrix. In addition, we also make the standard assumption that $\mathrm{Tr}[\hat{B}(t)\hat{\rho}_B] = 0$ [48]. The system dynamics becomes

$$\begin{aligned}\frac{d}{dt}\hat{\rho}(t) &= -\mathrm{Tr}_B\left[\hat{H}(t), \int_0^t [\hat{H}(t-\tau), \hat{\rho}(t-\tau) \otimes \hat{\rho}_B]d\tau\right] \\ &= \int_0^t [\hat{O}(t-\tau)\hat{\rho}(t-\tau)\hat{O}(t) \\ &\quad - \hat{O}(t)\hat{O}(t-\tau)\hat{\rho}(t-\tau)] \\ &\quad \times C_B(t, t-\tau)d\tau + \mathrm{H.c.}, \end{aligned} \tag{A2}$$

where we define the two-point correlation functions

$$\begin{aligned}C_B(t, t-\tau) &= \langle \hat{B}(t)\hat{B}(t-\tau)\rangle \\ &= \mathrm{Tr}_B[\hat{B}(t)\hat{B}(t-\tau)\hat{\rho}_B] = C_B(t-\tau, t)^*. \end{aligned} \tag{A3}$$

To proceed, we assume that the bath is stationary with a very short correlation decay time. In other words,

$$C_B(t, t-\tau) = C_B(\tau, 0) \equiv C_B(\tau) \sim e^{-\tau/\tau_B}, \tag{A4}$$

where τ_B is much shorter than any timescale we are interested in. Assuming weak system-bath coupling, we have $|\hat{O}(t) - \hat{O}(t-\tau_B)| \sim |\hat{O}|$ and $|\hat{\rho}(t) - \hat{\rho}(t-\tau_B)| \sim |\hat{O}|^2$, which is second order in the coupling strength. Therefore, we could make the Markov approximation and replace $\hat{\rho}(t-\tau)$ with $\hat{\rho}(t)$ in Eq. (A2). Since only $\tau \approx 0$ contributes significantly to the integration, the upper limit of the integration can be extended to ∞:

$$\begin{aligned}\frac{d}{dt}\hat{\rho}(t) &= \int_0^\infty [\hat{O}(t-\tau)\hat{\rho}(t)\hat{O}(t) - \hat{O}(t)\hat{O}(t-\tau)\hat{\rho}(t)] \\ &\quad \times C_B(\tau)d\tau + \mathrm{H.c.} \end{aligned} \tag{A5}$$

For Floquet systems, we have $\hat{O}(t) = \sum_\omega \hat{O}(\omega)e^{-i\omega t}$ with $\hat{O}(\omega) = \hat{O}^\dagger(-\omega)$ since $\hat{O}(t)$ is Hermitian. Therefore,

$$\int_0^\infty \hat{O}(t-\tau)C_B(\tau)d\tau = \sum_\omega \hat{O}(\omega)e^{-i\omega t}\Gamma(\omega), \tag{A6}$$

where

$$\Gamma(\omega) = \int_0^\infty e^{i\omega\tau}C_B(\tau)d\tau. \tag{A7}$$

We could decompose $\Gamma(\omega)$ into its real and imaginary parts as $\Gamma(\omega) = \frac{1}{2}\gamma(\omega) + iS(\omega)$, where

$$\begin{aligned}\gamma(\omega) &= \int_{-\infty}^\infty e^{i\omega\tau}C_B(\tau)d\tau, \\ S(\omega) &= \int_{-\infty}^\infty \frac{d\omega'}{2\pi}\gamma(\omega')\mathcal{P}\left(\frac{1}{\omega-\omega'}\right). \end{aligned} \tag{A8}$$

Physically, the real part $\gamma(\omega)$ represents the decay rate while the imaginary part $S(\omega)$ can be absorbed into the system Hamiltonian, which we will ignore for now.

Consider a zero-temperature bath with a flat spectral density function

$$\gamma(\omega) = \begin{cases}\gamma, & \omega > 0 \\ 0, & \omega \leqslant 0\end{cases} \tag{A9}$$

as an example. We could decompose $\hat{O}(t)$ into positive- and negative-frequency parts where

$$\hat{O}_+(t) = \sum_{\omega<0}\hat{O}(\omega)e^{-i\omega t}, \quad \hat{O}_-(t) = \sum_{\omega>0}\hat{O}(\omega)e^{-i\omega t}, \tag{A10}$$

and $\hat{O}_+(t) = \hat{O}_-^\dagger(t)$. Therefore,

$$\int_0^\infty \hat{O}(t-\tau)C_B(\tau)d\tau = \frac{\gamma}{2}\sum_{\omega>0}\hat{O}(\omega)e^{-i\omega t} = \frac{\gamma}{2}\hat{O}_-(t) \tag{A11}$$

and Eq. (A5) gives the Floquet master equation

$$\begin{aligned}\frac{d}{dt}\hat{\rho}(t) &= \frac{\gamma}{2}\hat{O}_-(t)\hat{\rho}(t)\hat{O}(t) - \frac{\gamma}{2}\hat{O}(t)\hat{O}_-(t)\hat{\rho}(t) + \mathrm{H.c.} \\ &= \gamma D[\hat{O}_-(t)]\hat{\rho}(t), \end{aligned} \tag{A12}$$

where we apply the RWA to drop $\hat{O}_\pm^2(t)$ terms. This justifies the Kapitzonium dissipator (17) in the main text.

APPENDIX B: GATE SIMULATION

1. Average gate fidelity

We benchmark the Kapitzonium gates with the measure of average fidelity $\bar{F}$ [49,50]. Intuitively, $\bar{F}$ describes how well the qubit subspace is preserved under some quantum process. More specifically, the average fidelity of a quantum channel

$\mathcal{M}$ over all states $|\psi\rangle = \sum_{n=1}^{N} c_n|n\rangle$ in an N-dimensional qubit subspace is

$$\bar{F} = \int d\psi \, \mathrm{Tr}[\mathcal{M}(|\psi\rangle\langle\psi|)|\psi\rangle\langle\psi|] = \sum_{mn} \mathrm{Tr}[\mathcal{M}(|m\rangle\langle n|)\rho_{mn}], \tag{B1}$$

where

$$\rho_{mn} = \int d\psi \, c_m c_n^* |\psi\rangle\langle\psi| = \sum_{kl} |k\rangle\langle l| \int d\psi \, c_m c_n^* c_k c_l^* = \delta_{mn}\left(\frac{2}{N(N+1)}|n\rangle\langle n| + \sum_{k\neq n}\frac{1}{N(N+1)}|k\rangle\langle k|\right) + (1-\delta_{mn})\frac{1}{N(N+1)}|n\rangle\langle m|. \tag{B2}$$

Therefore, the average fidelity can be simplified as

$$\bar{F} = \frac{1}{N(N+1)}\sum_n \mathrm{Tr}\left(\mathcal{M}(|n\rangle\langle n|)\sum_k (1+\delta_{nk})|k\rangle\langle k|\right) + \frac{2}{N(N+1)}\sum_{m<n}\mathrm{Re}\{\mathrm{Tr}[\mathcal{M}(|m\rangle\langle n|)|n\rangle\langle m|]\}. \tag{B3}$$

To compare $\mathcal{M}$ with some target unitary $\hat{U}$, we could compare $\mathcal{M}'$ with identity instead, where $\mathcal{M}'(\hat{\rho}) \equiv \hat{U}^\dagger \mathcal{M}(\hat{\rho})\hat{U}$.

2. Unitary case

The gates are designed such that the system Hamiltonian adiabatically evolves from the idling $\hat{H}_0(t)$ to the gate Hamiltonian $\hat{H}_{\mathrm{gate}}(t)$ and then adiabatically evolves back to $\hat{H}_0(t)$ after a certain amount of gate time. The average gate fidelity is calculated for the single-qubit subspace with $N = 2$ or the two-qubit subspace with $N = 4$. We choose the pulse shape

$$\alpha(t, t_{\mathrm{gate}}, \tau) = \begin{cases} \sin\left(\frac{\pi t}{2\tau}\right)^2, & 0 \leqslant t < \tau \\ 1, & \tau \leqslant t \leqslant t_{\mathrm{gate}} - \tau \\ \sin\left(\frac{\pi (t_{\mathrm{gate}} - t)}{2\tau}\right)^2, & t_{\mathrm{gate}} - \tau < t \leqslant t_{\mathrm{gate}}, \end{cases} \tag{B4}$$

where t_{gate} is the total gate duration and τ is the adiabatic ramping time.

a. The X gate

The Hamiltonian is

$$\hat{H}_x(t) = \hat{H}_0(t) + \alpha_x \alpha(t, t_x, \tau_x)\cos\hat{\phi}, \tag{B5}$$

where $t_x = 60$ ns, $\tau_x = 10$ ns, and $\alpha_x/2\pi \approx 5.2$ MHz. The X gate implements the mapping of $|\Psi_0\rangle \to |\Psi_1\rangle$ and $|\Psi_1\rangle \to |\Psi_0\rangle$ with an infidelity of 1.7×10^{-7}.

b. The Z gate

The Hamiltonian is

$$\hat{H}_z(t) = 4E_C\hat{n}^2 - E_J\alpha_z(t)\cos\hat{\phi}, \tag{B6}$$

where

$$\alpha_z(t) = [1 - \alpha(t, t_z, \tau_z)]\cos\omega t + \alpha(t, t_z, \tau_z)\cos\omega_z t. \tag{B7}$$

We choose $t_z = 296.2$ ns, $\tau_z = 20$ ns, and $\omega_z/2\pi = 20$ GHz. The Z gate implements the mapping of $|\Psi_0\rangle \to |\Psi_0\rangle$ and $|\Psi_1\rangle \to -|\Psi_1\rangle$ with an infidelity of 4.6×10^{-6}.

Another Floquet drive that seems reasonable at first is to have frequency modulation instead of amplitude modulation:

$$\alpha_z(t) = \cos\{[(1 - \alpha(t, t_z, \tau_z)]\omega + \alpha(t, t_z, \tau_z)\omega_z]t\}. \tag{B8}$$

However, this Floquet drive always leads to unstable dynamics which heats up the Kapitzonium even with very slow ramping.

c. The XX gate

The Hamiltonian is

$$\hat{H}_{xx}(t) = \hat{H}_0^{(1)}(t) + \hat{H}_0^{(2)}(t) + \alpha_{xx}\alpha(t, t_{xx}, \tau_{xx})\cos(\hat{\phi}_1 - \hat{\phi}_2), \tag{B9}$$

where $\hat{H}_0^{(i)}(t) = 4E_C\hat{n}_i^2 - E_J\cos\omega t\cos\hat{\phi}_i$ is the idling Hamiltonian for each qubit with $i = 1, 2$. We choose $t_{xx} = 39$ ns, $\tau_{xx} = 12$ ns, and $\alpha_{xx}/2\pi = 10$ MHz. The XX gate implements the mapping of $|\Psi_0\Psi_0\rangle \to |\Psi_1\Psi_1\rangle$, $|\Psi_0\Psi_1\rangle \to |\Psi_1\Psi_0\rangle$, $|\Psi_1\Psi_0\rangle \to |\Psi_0\Psi_1\rangle$, and $|\Psi_1\Psi_1\rangle \to |\Psi_0\Psi_0\rangle$ with an infidelity of 2.4×10^{-7}.

d. State initialization

To initialize the system state into $|0\rangle$, we could start from the ground state of the static transmon Hamiltonian $\hat{H} = 4E_C\hat{n}^2 - E_J\cos\hat{\phi}$ and adiabatically apply the Floquet drive

$$\hat{H}(t) = 4E_C\hat{n}^2 - E_J\{\alpha(t)\cos\omega t + [1 - \alpha(t)]\}\cos\hat{\phi}, \tag{B10}$$

where $\alpha(t)$ increases from 0 to 1.

3. Open system without a filter

In the open-system simulation without a filter, the Floquet drives are identical to the unitary case. The only difference is that during $t \in [\tau, t_{\mathrm{gate}} - \tau]$ we add loss to the system. More specifically, the simulation is performed in the interaction picture with Hamiltonian 0 and a single Lindblad dissipator $\kappa D[\hat{O}_-(t)]$. Notice that the interaction picture here is defined with respect to $\hat{H}_{\mathrm{gate}}(t)$ instead $\hat{H}_0(t)$.

During the ramping parts of the Floquet drive, the Hamiltonian is not strictly time periodic, which makes it difficult to calculate the time-dependent dissipator. Therefore, the ramping parts are always assumed to be unitary and the simulation is done in the laboratory frame.

4. Open system with a filter

Due to the hybridization between the Kapitzonium and the filter, $|\Psi_\alpha(t)\rangle \otimes |0_f\rangle$ is no longer the Floquet eigenstates of the full Hamiltonian (23), where $|0_f\rangle$ is the ground state of the filter. Therefore, we work with the dressed Floquet eigenstates $|\widetilde{\Psi_\alpha(t)}\rangle$ of Eq. (23) instead. The qubit basis states $\{|\widetilde{\Psi_0(t)}\rangle, |\widetilde{\Psi_1(t)}\rangle\}$ are chosen based on their overlap with $\{|\Psi_0(t)\rangle \otimes |0_f\rangle, |\Psi_1(t)\rangle \otimes |0_f\rangle\}$.

The Floquet drive parameters require a slight fine-tuning due to this hybridization. During the gate time $t \in [\tau, t_{\mathrm{gate}} - \tau]$, the simulation is performed in the interaction picture

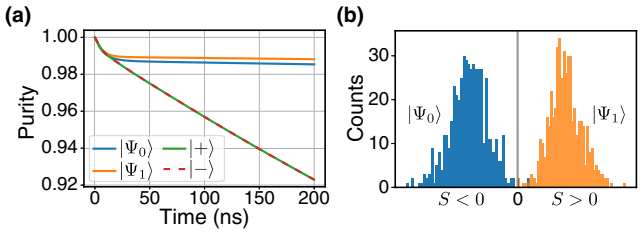

FIG. 5. (a) The Z gate simulation with a filter for different initial states. (b) The Z measurement results.

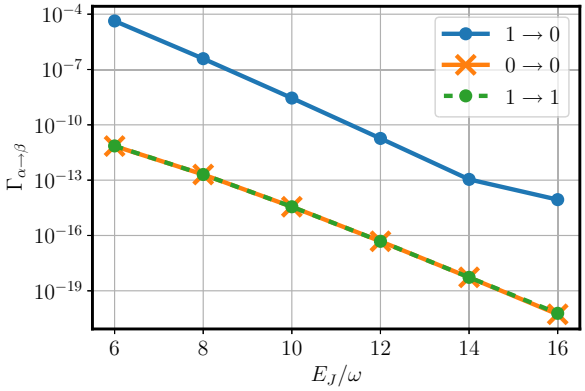

FIG. 6. Kapitzonium transition rates for $n_g = 0.3$. The junction energies are $E_J/2\pi = 60, 80, 100, 120, 140, 160$ GHz, with $\omega/2\pi = 10$ GHz and $E_C/2\pi = 0.01$ GHz fixed.

defined by $\hat{H}_{\text{gate}}(t)$ with Hamiltonian 0 and two Lindblad dissipators $\kappa D[\hat{O}_-(t)]$ and $\kappa_f D[\hat{a}_N(t)]$. Here $\hat{a}_N(t)$ is calculated similarly to Eq. (17) with $\hat{O} = \hat{a}_N + \hat{a}_N^\dagger$. To remove any transient effects at the beginning of the cooling [51], we prepare the initial states for benchmarking the gates by evolving the qubit basis states for 50 ns of idling until the system reaches equilibrium.

In Fig. 5(a) we simulate the unprotected Z gate for different initial states. Here $|\Psi_0\rangle$ and $|\Psi_1\rangle$ are the dressed Floquet eigenstates with $\omega/2\pi = 20$ GHz and $|\pm\rangle$ are their even and odd superpositions. We choose $\omega_f/2\pi \approx 20.234$ GHz, $\kappa_f/2\pi = 200$ MHz, $J = \kappa_f/2$, and $g = \kappa_f/5$ for the Z gate filter.

We use QUTIP [52,53] for all the simulations and modify the built-in `mesolve` function to speed up the open-system simulation with time-dependent dissipators.

APPENDIX C: MEASUREMENT SIMULATION

The full Hamiltonian including the charge drive and the filter modes for the measurement simulation is

$$\begin{aligned}\hat{H}(t) =& 2\Omega[\cos(\omega_{d1}t) + \cos(\omega_{d2}t)]\hat{n}(t) \\ &+ g\hat{n}(t)(\hat{a}_1 e^{-i\omega_f t} + \hat{a}_1^\dagger e^{i\omega_f t}) \\ &+ J\sum_{k=1}^{N-1}(\hat{a}_k\hat{a}_{k+1}^\dagger + \hat{a}_k^\dagger\hat{a}_{k+1}),\end{aligned} \tag{C1}$$

which is in the interaction picture of the measurement Hamiltonian $\hat{H}_{\text{meas}}(t)$ and the rotating frame of the filter modes. Note that the simulation only includes the first four Floquet eigenstates with $\hat{n}(t)$ in Eq. (24) represented by a 4×4 matrix.

For the X measurement, we choose $\hat{H}_{\text{meas}}(t) = \hat{H}_0(t) + \alpha_x\cos\hat{\phi}$, with $\alpha_x/2\pi = 500$ MHz, and calculate $\hat{n}(t)$ from the emission spectrum of $\hat{H}_{\text{meas}}(t)$. The charge drive frequencies are $\omega_{02}/2\pi \approx 9.44$ GHz and $\omega_{13}/2\pi \approx 9.52$ GHz. The emitted photon frequencies are $\omega_{20}/2\pi \approx 10.56$ GHz and $\omega_{31}/2\pi \approx 10.48$ GHz. We choose $\Omega/2\pi = 6.4$ MHz and the filter parameters g, J, and ω_f are the same as for the idling filter.

For the Z measurement, $\hat{H}_{\text{meas}}(t)$ is the same as for the Z gate. The charge drive frequencies are $\omega_{02}/2\pi \approx 19.78$ GHz and $\omega_{13}/2\pi \approx 19.75$ GHz. The emitted photon frequencies are $\omega_{20}/2\pi \approx 20.22$ GHz and $\omega_{31}/2\pi \approx 20.25$ GHz. We choose $\Omega/2\pi = 2.3$ MHz and the filter parameters are the same as for the Z gate filter. Starting from the initial state $(|\Psi_0\rangle + |\Psi_1\rangle)/\sqrt{2}$, we simulate 1000 trajectories for the Z measurement with a measurement time of 10 μs [Fig. 5(b)] and the measurement fidelity is about 99.8%.

We would like to make a few comments on Kapitzonium measurement. First, the charge drive could be slightly off-resonant from the heating transitions with $\omega_{d1} \approx \omega_{02}$ and $\omega_{d2} \approx \omega_{13}$, which shifts the emitted photon frequencies as well. Second, the charge drive frequency should be outside the filter passband. In principle, setting $\omega_{d1} \approx \omega_{20}$ and $\omega_{d2} \approx \omega_{13}$ also drives the Rabi oscillation via the cooling transitions. However, this could cause measurement error if there is any direct leakage from the charge drive to the output of the filter. Finally, choosing Ω to be comparable to or larger than Δ will cause measurement error due to crosstalk between the drives. On the other hand, a very small Ω reduces the measurement rate and requires a long measurement time.

APPENDIX D: KAPITZONIUM LIFETIME ESTIMATION

The Kapitzonium Hamiltonian in the presence of offset charge n_g is

$$\hat{H}_0(t) = 4E_C(\hat{n} - n_g)^2 - E_J\cos\omega t\cos\hat{\phi}. \tag{D1}$$

For $n_g \neq 0$, $\hat{H}_0(t)$ does not have the symmetry under $\hat{\Pi}_1$ and the bit-flip and phase-flip rates are no longer exactly 0 (see Sec. III A). However, since the Kapitzonium is in the deep-potential-well regime $E_J/\omega \gg 1$, we still expect the Floquet eigenstates to be insensitive to n_g. We define the total transition rate from $|\Psi_\alpha\rangle$ to $|\Psi_\beta\rangle$ as

$$\Gamma_{\alpha\to\beta} \equiv \sum_{\varepsilon_\alpha - \varepsilon_\beta + n\omega > 0} |O_{\alpha\beta n}|^2, \tag{D2}$$

where $1/T_1 \sim \Gamma_{1\to 0}$ and $1/T_2 \sim \Gamma_{0\to 0}, \Gamma_{1\to 1}$. In Fig. 6 we plot the transition rates for different values of E_J/ω at $n_g = 0.3$. The results indeed show an exponential suppression of both the bit-flip and phase-flip rates with E_J/ω.

[1] A. Blais, A. L. Grimsmo, S. M. Girvin, and A. Wallraff, Rev. Mod. Phys. **93**, 025005 (2021).

[2] M. Kjaergaard, M. E. Schwartz, J. Braumüller, P. Krantz, J. I.-J. Wang, S. Gustavsson, and W. D. Oliver, Annu. Rev. Condens. Matter Phys. **11**, 369 (2020).

[3] J. Koch, T. M. Yu, J. Gambetta, A. A. Houck, D. I. Schuster, J. Majer, A. Blais, M. H. Devoret, S. M. Girvin, and R. J. Schoelkopf, Phys. Rev. A **76**, 042319 (2007).

[4] V. E. Manucharyan, J. Koch, L. I. Glazman, and M. H. Devoret, Science **326**, 113 (2009).

[5] P. Brooks, A. Kitaev, and J. Preskill, Phys. Rev. A **87**, 052306 (2013).

[6] A. Gyenis, A. Di Paolo, J. Koch, A. Blais, A. A. Houck, and D. I. Schuster, PRX Quantum **2**, 030101 (2021).

[7] K. Kalashnikov, W. T. Hsieh, W. Zhang, W.-S. Lu, P. Kamenov, A. Di Paolo, A. Blais, M. E. Gershenson, and M. Bell, PRX Quantum **1**, 010307 (2020).

[8] I. V. Pechenezhskiy, R. A. Mencia, L. B. Nguyen, Y.-H. Lin, and V. E. Manucharyan, Nature (London) **585**, 368 (2020).

[9] N. Ofek, A. Petrenko, R. Heeres, P. Reinhold, Z. Leghtas, B. Vlastakis, Y. Liu, L. Frunzio, S. M. Girvin, L. Jiang, M. Mirrahimi, M. H. Devoret, and R. J. Schoelkopf, Nature (London) **536**, 441 (2016).

[10] L. Hu, Y. Ma, W. Cai, X. Mu, Y. Xu, W. Wang, Y. Wu, H. Wang, Y. P. Song, C.-L. Zou, S. M. Girvin, L.-M. Duan, and L. Sun, Nat. Phys. **15**, 503 (2019).

[11] P. Campagne-Ibarcq, A. Eickbusch, S. Touzard, E. Zalys-Geller, N. E. Frattini, V. V. Sivak, P. Reinhold, S. Puri, S. Shankar, R. J. Schoelkopf, L. Frunzio, M. Mirrahimi, and M. H. Devoret, Nature (London) **584**, 368 (2020).

[12] P. Groszkowski, A. D. Paolo, A. L. Grimsmo, A. Blais, D. I. Schuster, A. A. Houck, and J. Koch, New J. Phys. **20**, 043053 (2018).

[13] A. Gyenis, P. S. Mundada, A. Di Paolo, T. M. Hazard, X. You, D. I. Schuster, J. Koch, A. Blais, and A. A. Houck, PRX Quantum **2**, 010339 (2021).

[14] M. Mirrahimi, Z. Leghtas, V. V. Albert, S. Touzard, R. J. Schoelkopf, L. Jiang, and M. H. Devoret, New J. Phys. **16**, 045014 (2014).

[15] Z. Leghtas, S. Touzard, I. M. Pop, A. Kou, B. Vlastakis, A. Petrenko, K. M. Sliwa, A. Narla, S. Shankar, M. J. Hatridge, M. Reagor, L. Frunzio, R. J. Schoelkopf, M. Mirrahimi, and M. H. Devoret, Science **347**, 853 (2015).

[16] R. Lescanne, M. Villiers, T. Peronnin, A. Sarlette, M. Delbecq, B. Huard, T. Kontos, M. Mirrahimi, and Z. Leghtas, Nat. Phys. **16**, 509 (2020).

[17] S. Puri, S. Boutin, and A. Blais, npj Quantum Inf. **3**, 18 (2017).

[18] A. Grimm, N. E. Frattini, S. Puri, S. O. Mundhada, S. Touzard, M. Mirrahimi, S. M. Girvin, S. Shankar, and M. H. Devoret, Nature (London) **584**, 205 (2020).

[19] E. Kapit, Phys. Rev. Lett. **116**, 150501 (2016).

[20] Z. Li, T. Roy, D. R. Pérez, K.-H. Lee, E. Kapit, and D. I. Schuster, Autonomous error correction of a single logical qubit using two transmons, Nat. Commun. **15**, 1681 (2024).

[21] L.-A. Sellem, A. Sarlette, Z. Leghtas, M. Mirrahimi, P. Rouchon, and P. Campagne-Ibarcq, A GKP qubit protected by dissipation in a high-impedance superconducting circuit driven by a microwave frequency comb, arXiv:2304.01425.

[22] A. Eckardt, Rev. Mod. Phys. **89**, 011004 (2017).

[23] J. Venkatraman, X. Xiao, R. G. Cortiñas, A. Eickbusch, and M. H. Devoret, Phys. Rev. Lett. **129**, 100601 (2022).

[24] N. Didier, E. A. Sete, J. Combes, and M. P. da Silva, Phys. Rev. Appl. **12**, 054015 (2019).

[25] Z. Huang, P. S. Mundada, A. Gyenis, D. I. Schuster, A. A. Houck, and J. Koch, Phys. Rev. Appl. **15**, 034065 (2021).

[26] A. Gandon, C. Le Calonnec, R. Shillito, A. Petrescu, and A. Blais, Phys. Rev. Appl. **17**, 064006 (2022).

[27] L. D. Landau and E. M. Lifshitz, *Mechanics*, 3rd ed. (Pergamon, Oxford, 1976), Vol. 1.

[28] U. Vool and M. Devoret, Int. J. Circuit Theory Appl. **45**, 897 (2017).

[29] X. You, J. A. Sauls, and J. Koch, Phys. Rev. B **99**, 174512 (2019).

[30] T. Rajabzadeh, Z. Wang, N. Lee, T. Makihara, Y. Guo, and A. H. Safavi-Naeini, Quantum **7**, 1118 (2023).

[31] S. P. Chitta, T. Zhao, Z. Huang, I. Mondragon-Shem, and J. Koch, New J. Phys. **24**, 103020 (2022).

[32] K. W. Murch, U. Vool, D. Zhou, S. J. Weber, S. M. Girvin, and I. Siddiqi, Phys. Rev. Lett. **109**, 183602 (2012).

[33] H. Putterman, J. Iverson, Q. Xu, L. Jiang, O. Painter, F. G. S. L. Brandão, and K. Noh, Phys. Rev. Lett. **128**, 110502 (2022).

[34] F. Reiter and A. S. Sørensen, Phys. Rev. A **85**, 032111 (2012).

[35] C. Chamberland, K. Noh, P. Arrangoiz-Arriola, E. T. Campbell, C. T. Hann, J. Iverson, H. Putterman, T. C. Bohdanowicz, S. T. Flammia, A. Keller, G. Refael, J. Preskill, L. Jiang, A. H. Safavi-Naeini, O. Painter, and F. G. S. L. Brandão, PRX Quantum **3**, 010329 (2022).

[36] H. M. Wiseman and G. J. Milburn, *Quantum Measurement and Control*, 1st ed. (Cambridge University Press, Cambridge, 2009).

[37] R.-P. Riwar and D. P. DiVincenzo, npj Quantum Inf. **8**, 36 (2022).

[38] D. Ristè, C. C. Bultink, M. J. Tiggelman, R. N. Schouten, K. W. Lehnert, and L. DiCarlo, Nat. Commun. **4**, 1913 (2013).

[39] K. Serniak, S. Diamond, M. Hays, V. Fatemi, S. Shankar, L. Frunzio, R. J. Schoelkopf, and M. H. Devoret, Phys. Rev. Appl. **12**, 014052 (2019).

[40] R. Lutchyn, L. Glazman, and A. Larkin, Phys. Rev. B **72**, 014517 (2005).

[41] R. M. Lutchyn, L. I. Glazman, and A. I. Larkin, Phys. Rev. B **74**, 064515 (2006).

[42] J. M. Martinis, M. Ansmann, and J. Aumentado, Phys. Rev. Lett. **103**, 097002 (2009).

[43] G. Catelani, J. Koch, L. Frunzio, R. J. Schoelkopf, M. H. Devoret, and L. I. Glazman, Phys. Rev. Lett. **106**, 077002 (2011).

[44] K. Serniak, M. Hays, G. de Lange, S. Diamond, S. Shankar, L. D. Burkhart, L. Frunzio, M. Houzet, and M. H. Devoret, Phys. Rev. Lett. **121**, 157701 (2018).

[45] M. Houzet, K. Serniak, G. Catelani, M. H. Devoret, and L. I. Glazman, Phys. Rev. Lett. **123**, 107704 (2019).

[46] D. Willsch, D. Rieger, P. Winkel, M. Willsch, C. Dickel, J. Krause, Y. Ando, R. Lescanne, Z. Leghtas, N. T. Bronn, P. Deb, O. Lanes, Z. K. Minev, B. Dennig, S. Geisert, S. Günzler, S. Ihssen, P. Paluch, T. Reisinger, R. Hanna *et al.*, Observation of Josephson harmonics in tunnel junctions, Nat. Phys. (2024), doi:10.1038/s41567-024-02400-8.

[47] M. Grifoni and P. Hänggi, Phys. Rep. **304**, 229 (1998).
[48] D. Manzano, AIP Adv. **10**, 025106 (2020).
[49] M. A. Nielsen, Phys. Lett. A **303**, 249 (2002).
[50] Z. Wang, T. Rajabzadeh, N. Lee, and A. H. Safavi-Naeini, PRX Quantum **3**, 020302 (2022).
[51] E. Kapit, Phys. Rev. Lett. **120**, 050503 (2018).
[52] J. Johansson, P. Nation, and F. Nori, Comput. Phys. Commun. **183**, 1760 (2012).
[53] J. R. Johansson, P. D. Nation, and F. Nori, Comput. Phys. Commun. **184**, 1234 (2013).